JOURNAL OF PROPULSION AND POWER
Vol. 14, No. 4, July–August 1998

Modified Fracture Mechanics Approach in Structural Analysis of Solid-Rocket Motors

Sook-Ying Ho*
Aeronautical and Maritime Research Laboratory, Salisbury SA 5108, Australia
and
Gerard Carè†
G+D Computing Pty. Ltd., Sydney NSW 2000, Australia

A deficiency in current failure initiation criteria used in the structural design and service-life prediction of solid-rocket motors, where the critical failure mode is structural failure, is the uncertainties associated with the criteria used in predicting crack initiation and propagation. Also, the constitutive models that describe the propellants' nonlinear behavior require an extensive experimental testing program to characterize the softening functions. A modified fracture mechanics method that accounts for bulk inelastic behavior in the calculation of a critical strain energy release rate and a relatively simple method for nonlinear viscoelastic analysis, where a three-dimensional interpolation scheme is used to solve the Prony series equations that represent Young's and shear relaxation moduli as functions of time, temperature, and strain level, have been developed and implemented into a finite element code. Predictions for a thermal shock loading on an end-burning research and development motor were made using the fracture mechanics and nonlinear viscoelastic analysis capabilities developed in this study. Reasonable agreement between the measured stresses from instrumented rocket motors and the predicted von Mises stresses was obtained. The regions of high propensity for crack propagation corresponded to the critical regions of maximum tensile principal stress in the motor.

Nomenclature

a = initial crack length
a_m = minimum crack size that will propagate with the local strain energy and material properties (from fracture mechanics/finite element analysis)
b = specimen thickness
e_c = critical strain for crack propagation
F = work done by the external force
G = strain energy release rate
G_c = fracture energy
H_r = hysteresis energy loss
K_c = critical stress intensity factor
K_{c1} = value of K_c for a state of plane strain
K_{c2} = value of K_c for a state of plane stress
l = specimen length
T_g = glass transition temperature
U = elastic stored energy in the bulk specimen
W_i = input strain energy density
W_{rc} = recoverable strain energy density
γ = surface free energy
∂A = increase in surface area associated with an increment of crack growth

Introduction

AT the present time the service life of solid-composite-propellant rocket motors can be predicted with a reasonable degree of confidence using service-life methodologies, such as the probabilistic approach,[1] cumulative damage model,[2] structural analysis approach,[3] etc. All of these methods require accurate stress predictions of the motor under the expected environmental (thermal loads during storage and operation) and operating (ignition pressurization and launch acceleration loads) conditions. Solid-rocket propellants exhibit significant nonlinear viscoelastic response and this has to be taken into account in the stress analysis. Until recently nonlinear constitutive models were not readily available and a great deal of effort is required to characterize the softening functions in these models to predict the propellants' nonlinear behavior.[4–6]

Another critical factor that determines the accuracy of the service-life prediction of rocket motors where the determining failure mode is structural failure, i.e., grain cracking or debonding, is the failure criteria used.[7] The propellant grain often contain flaws/defects in the form of microcracks and voids, etc. (which are introduced during manufacture), from which cracks can initiate and propagate under suitable conditions. Current failure initiation criteria used in the structural design and service-life prediction of many tactical motors predict failure when a crack is initiated. However, failure criteria based only on crack initiation are often inadequate. These criteria underpredict service life and result in the early withdrawal of motors from service, which is very wasteful because rocket motors are expensive service items. Experiments in this and other laboratories have shown that rocket motors with small cracks or debonds may still statically fire without catastrophic failure or without showing unacceptable ballistic performance.[8,9] In the past, crack propagation was not considered in the structural analysis of solid-propellant grains, even though this problem is widely recognized, because of the uncertainties in the failure criteria used and the difficulty in implementing the J-integral (or crack extension force) method into the structural analysis, which is commonly used in fracture mechanics to predict plastic crack propagation.

In the present study a modified fracture mechanics approach,[7] where bulk inelastic behavior is accounted for in the calculation of the fracture energy G_c, is implemented into a commercial general-purpose finite element code, STRAND 6, to predict the critical or minimum crack length above which

Received Jan. 30, 1997; revision received Oct. 1, 1997; accepted for publication Feb. 5, 1998. Copyright © 1998 by the American Institute of Aeronautics and Astronautics, Inc. All rights reserved.

*Principal Research Scientist.
†Chief Engineer.

crack propagation occurs, i.e., propensity for crack propagation, in a rocket motor under typical service-life thermal loadings. Because G_c indicates the energy required for crack extension, it should be a more appropriate failure criterion than criteria based on stress or strain capabilities alone. The time-temperature dependence of the fracture behavior of the propellant is modeled by employing a time–temperature-dependent modulus. A relatively simple method for nonlinear viscoelastic analysis was developed by implementing a three-dimensional interpolation scheme in the finite element analysis to solve the Prony series equations (representing the relaxation modulus) for the displacements, stresses and strains, taking into account the time, temperature, and strain-dependent variation of the material properties.

Modified Fracture Mechanics Approach for Inelastic Crack Propagation

Solid-composite rocket propellants undergo bulk inelastic behavior, such as viscous and plastic deformation, and dewetting or unbonding of the crystalline oxidizer particles from the polymeric binder. Thus, such materials exhibit loading and unloading characteristics where mechanical hysteresis occurs, i.e., only a portion of the applied strain energy is recoverable and, therefore, linear elastic fracture mechanics (LEFM) cannot be applied to these materials to predict crack propagation.

A fracture mechanics analysis whereby bulk inelastic behavior is allowed for in the calculation of the fracture energy has been reported previously.[7,10] This approach is an extension of the Griffith's theory, where an energy criterion for fracture is used to describe crack propagation by the following equation:

$$\frac{\partial}{\partial a}(F - U) \geq \gamma \frac{\partial A}{\partial a} \tag{1}$$

where ∂A is the increase in surface area associated with an increment of crack growth ∂a. Assuming that the energy dissipation around the crack tip occurs in a manner independent of test geometry and loading conditions, 2γ may be replaced by G_c, the energy required to increase the crack by unit length.

The fracture energy approach can be readily extended to inelastic materials.[11] In these materials crack growth always involves plastic flow and viscoelastic dissipation of energy, resulting in the energy required for crack growth to be much greater than 2γ. Thus, the fracture energy criterion for crack propagating in a sheet of thickness b is given by

$$\frac{1}{b}\left[\frac{\partial}{\partial a}(F - U)\right] \geq G_c \tag{2}$$

Here, G_c, the critical strain energy release rate, is the total amount of energy dissipated during crack growth and includes energy dissipated by plastic deformation and viscoelastic processes. The energy available for crack propagation is now taken as the input strain energy density minus the hysteresis (loss) energy.

This approach has been applied to solid propellants[7,10] for various specimen geometry and loading conditions. For a given specimen geometry and loading condition, an expression for G_c (which is a function of the applied stress, initial crack length, and a nondimensional function of the specimen dimension) can be obtained either analytically or numerically. Previous studies have confirmed the independence of G_c upon different geometries and types of loading, e.g., similar fracture energies were obtained from trouser test and single-edge notched (SEN) specimens.[7,10] Because the parameters defining G_c are true material parameters that are independent of test geometry and loading conditions, there is a considerable advantage of using this failure criterion over other methods in the structural analysis of rocket motors. However, G_c is dependent on temperature and strain rate, as expected from the viscoelastic nature of the propellant, and must be evaluated at the appropriate temperatures and strain rates seen by the motor during storage and operation.

In this study G_c was evaluated using a SEN geometry (consisting of a parallel-sided sheet of material containing a short, sharp-edge crack), given by the equation

$$G_c = 2\pi a W_{rc}/(1 + e_c)^{1/2} \tag{3}$$

At a given temperature and strain rate the value of W_{rc} can be evaluated by measuring W_i for crack growth and H_r (at the same temperature and strain rate) to allow for bulk inelastic behavior.[7] The value of H_r, i.e., (loading energy–unloading energy)/loading energy, is independent of the strain level[7] and, therefore, $W_{rc} = W_i(1 - H_r)$. However, H_r must be determined at the same time scale, i.e., strain rate, and temperature as those under which W_i was measured. Additionally, it has been shown that W_{rc} is linearly dependent on strain rate for several propellants studied[7] (in the strain-rate range 10^{-3}–10^{-5} s^{-1}) and, hence, the value of W_{rc} for the subsequent calculation of G_c at a given strain rate can be obtained by interpolation.

Although the variation of G_c with a strain rate appropriate to rocket-motor service-life storage conditions is relatively small, it was found that G_c at −40°C can be 1.2–1.5 times higher than the value at ambient temperature.[8,12] An input table of G_c vs temperature is being implemented in the DSTO version of the STRAND 6 finite element code for fracture analysis of materials, where the temperature effect is significant. In this study G_c was evaluated at ambient temperature (22°C) only, and it is assumed that it does not vary significantly over the temperature range used in the structural analysis.

It is sometimes found that the fracture energy varies with specimen thickness over a particular range of thicknesses[11,13] because of plane stress conditions (biaxial stress field) changing to plane strain conditions (triaxial stress field) for thick specimens. In very thin specimens K_c becomes equal to K_{c2}, whereas for very thick specimens $K_c \approx K_{c1}$. For example, it has been reported that K_c for a nitrocellulose/nitroglycerine-based (NC/NG) propellant (where LEFM is applicable) has a significant thickness effect at low temperatures.[13] For this NC/NG propellant, the difference between K_c values for 10- and 50-mm-thick specimens was ≈20% at 20°C and ≈40% at −60°C. Because G_c is related to K_c, the fracture energy may show a similar dependence on specimen thickness. The fracture energy may be corrected for thickness effect using empirical correction factors. In the present study it was assumed that plane strain conditions predominate in the test specimens and the rocket motor, and G_c does not vary significantly with the aspect ratio of the specimen.

Implementation of Fracture Energy and Nonlinear Viscoelastic Analysis into Finite Element Code

Implementation of the modified fracture mechanics approach described earlier and a three-dimensional interpolation scheme for nonlinear viscoelastic analysis into the DSTO version of the STRAND 6 code has been described elsewhere and is summarized next.[12,14] The new solvers in the code were benchmarked using coupon specimens loaded in tension and shear, and further validated using instrumented rocket motors (see the next section). The finite element code uses an iterative procedure to determine the time history of temperature and stress/strain distribution. This is a two-step process.

1) The temperature distribution as a function of time is calculated using a two-dimensional/three-dimensional potential flow solver.[15] Material properties, i.e., thermal conductivity, specific heat capacity, etc., can be dependent on temperature. The thermal loading is applied as a time-varying ambient tem-

perature condition to model the change in environment. This generates heat flow through the motor via appropriate convective and radiation coefficients on the surface of the motor. The standard equations governing heat transfer in the rocket motor and the heat transfer coefficients used in this analysis have been described in detail elsewhere.[14,15]

2) Using the temperature–time history calculated in the previous text, the Visco (Prony) analysis is conducted. An initial stiffness matrix is assembled and a time-stepping solution technique is applied. The stiffness matrix is periodically updated to take into account the changes in stiffness by interpolating the material moduli directly from the Prony curves and updating the loading because of the changing temperature distribution. The Prony curves give the moduli as a function of temperature, time, and strain.

The nodal displacements, stresses, and strains are postprocessed to calculate nodal values of recoverable strain energy and critical crack length as a function of time, using the modified fracture mechanics approach described earlier.

Crack propagation occurs when existing cracks in the propellant reach a certain crack length based on the state of strain energy and stress in the structure at any point, i.e., when $G \geq$ the critical strain energy release rate. The critical or minimum crack length above which propagation occurs a_m is calculated using the failure criterion given by Eq. (2), and is based on the measured G_c and H_r values at a particular temperature and the state of strain energy and stress in the structure.

Nonlinear Viscoelastic and Fracture Analysis of Solid-Rocket Motor

An Australian R&D motor (Fig. 1), Pictor, was used in the structural analysis to illustrate the nonlinear viscoelastic and crack propagation analysis developed in this and previous studies.[7] The finite element analysis was carried out on an axisymmetric model of the motor for a thermal loading that is typical of thermal shock environmental conditions used in the service-life assessment of rocket motors. The thermal transients in the thermal shock loading are defined next (Fig. 2): 1) Ambient (25°C) to −40°C; 2) 16 h at −40°C; 3) −40°C to ambient; 4) 8 h at ambient; 5) ambient to +60°C; 6) 16 h at +60°C; 7) +60°C to ambient; and 8) 8 h at ambient.

The structural analysis was also carried out using a three-dimensional solid brick model of a 10-deg wedge to check the

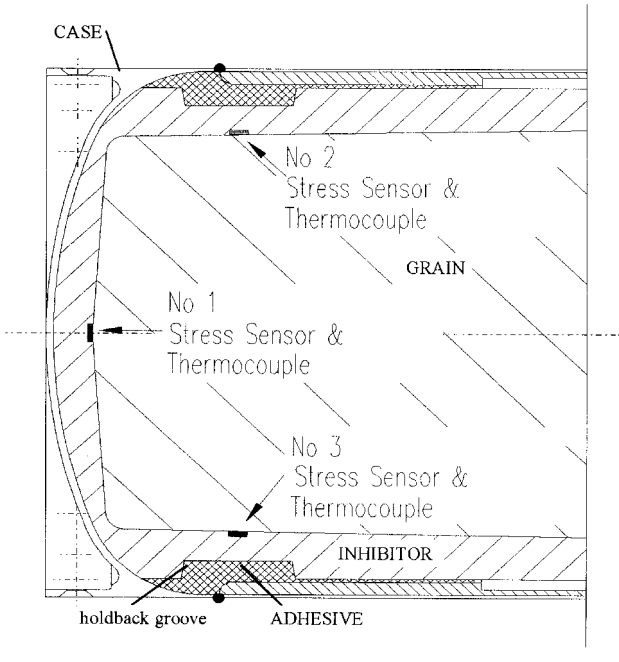

Fig. 1 Instrumented Pictor rocket motor.

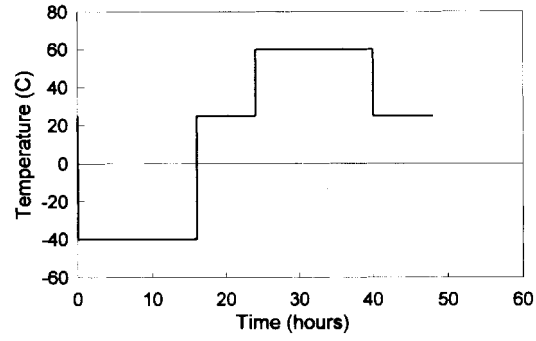

Fig. 2 Thermal transients for thermal shock loading.

accuracy of the code. The three-dimensional brick model showed almost the same results as those obtained from the axisymmetric model. Hence, all of the analyses were conducted using the axisymmetric model.

The viscoelastic solutions assume that the motor begins in a state of zero stress and strain at the start of the thermal loading at time zero. Thermal cooldown tests, using rocket motors instrumented with miniature normal stress sensors, showed that the stress-free temperature of this motor is ~55°C.[8,12] The residual stress (arising from the restriction of thermal contraction of the propellant on solidification when the cure temperature decreased from ≈60°C to ambient), measured at the critical regions of stress (see Fig. 1), at 25°C (equilibrium temperature at the start of the analysis) is ≈48 kPa. Thus, the predicted stresses would have to be corrected for residual stresses present in the motor at the starting equilibrium temperature. Alternatively, we could start the analysis at a steady-state ambient of 55°C, but rocket motors are not normally stored at this temperature.

Von Mises stress contours in the Pictor motor at the end of the downward (25 to −40°C) and upward (25 to +60°C) thermal transients are shown in Figs. 3a and 3b, respectively. The nonlinear viscoelastic analysis predicts that the high stresses in the propellant are concentrated at the head end of the motor and also at the side adjacent to the stiff adhesive in the holdback groove of the inhibitor. In the downward thermal transient, the von Mises stress in the propellant adjacent to the holdback groove of the inhibitor and near the head end of the motor is ~420 kPa (470 kPa after correction for residual stress in the motor at 25°C). This compares with the experimental values of 500 and 380 kPa, measured using miniature normal stress sensors embedded in the propellant grain at the side of the motor adjacent to the holdback groove of the inhibitor[8,12] (Fig. 1). In the upward thermal transient (25–60°C), the predicted stresses in the propellant are ≈140 kPa (190 kPa after correction) adjacent to the holdback groove of the inhibitor, and ≈110 kPa (160 kPa after correction) at the head end of the motor. This is in reasonable agreement with experimental values of 133 and 80 kPa measured from miniature stress sensors embedded in the propellant grain at the side of the motor (Fig. 1). The difference between the predicted and measured stresses and the reason for the stresses measured by the two sensors located symmetrically with respect to the axial axis of the motor not being equal can be attributed to 1) experimental errors of ±30% arising from stress gauge installation, calibration, corrections for temperature sensitivity and zero offsets of the transducers,[12] etc.; and 2) there may be defects such as microcracks and voids (not modeled in the stress analysis) in the propellant grain that are closer (radially) to one of the side sensors.

The maximum tensile principal stress distributions in the motor at the end of the downward and upward thermal transients are shown in Figs. 4a and 4b, respectively. In contrast to the von Mises stress distributions, the maximum tensile principal stress contours show critical regions at the corner of

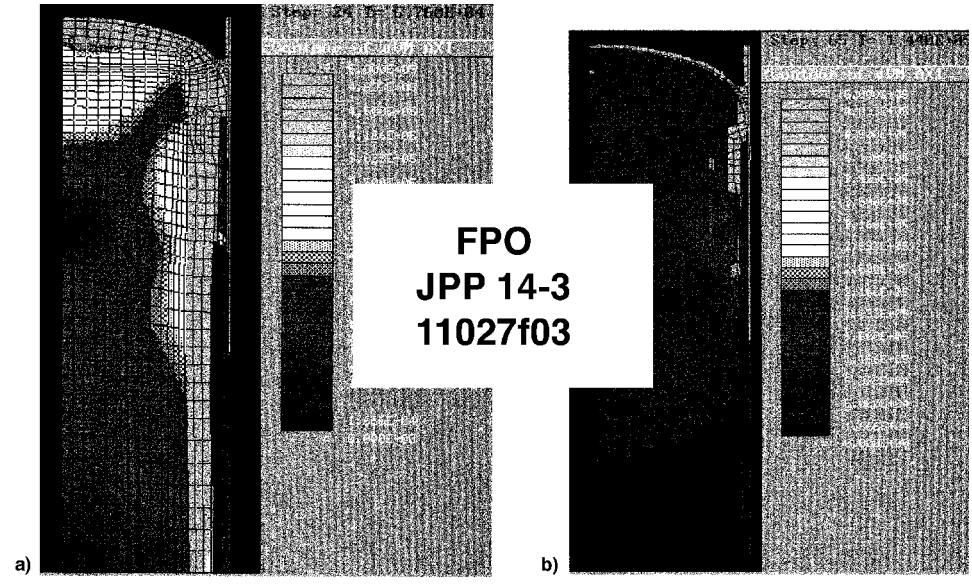

Fig. 3 Von Mises stress contours for a) end of downward (25 to −40°C) thermal transient and b) end of upward (25 to +60°C) thermal transient.

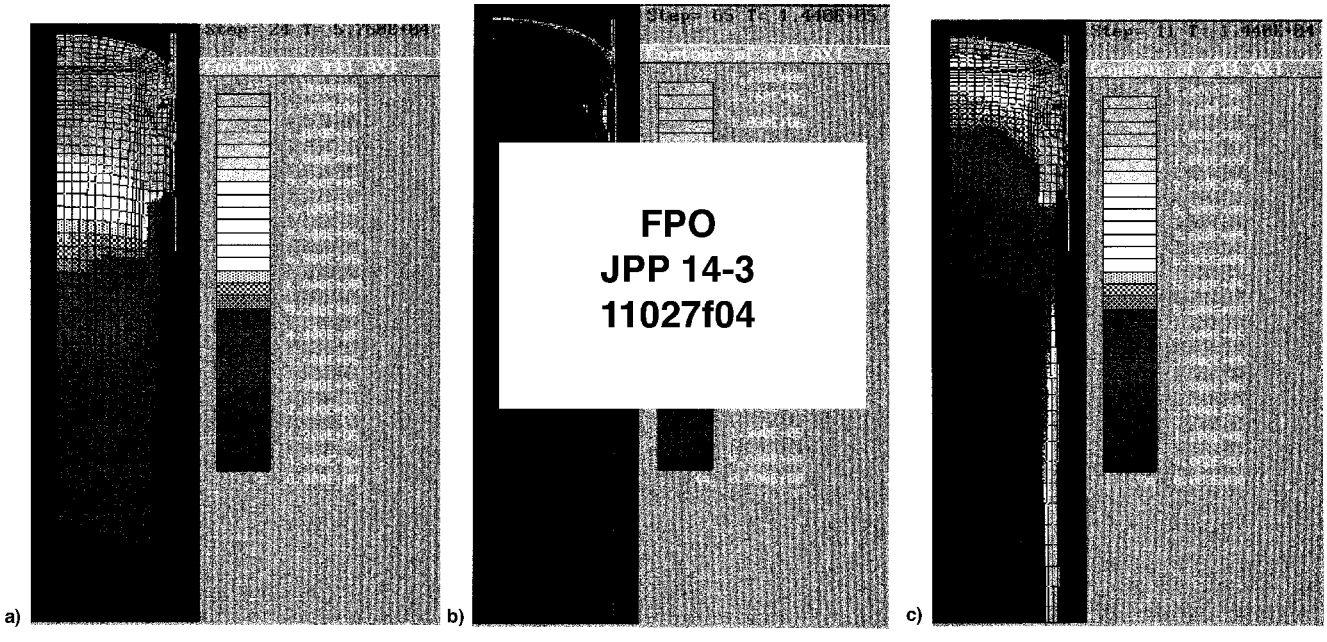

Fig. 4 Maximum tensile principal stress contours for a) end of downward (25 to −40°C) thermal transient, b) end of upward (25 to +60°C) thermal transient, and c) after 2.5 h at −40°C.

the dome at the head end of the motor. After approximately 2 h at −40°C (where the most rapid changes in temperature and, therefore, thermal stress occur), the predicted maximum tensile principal stresses in the propellant grain are 100 kPa at the corner and 60 kPa at the side and middle of the head end of the motor (Fig. 4c). The predicted maximum principal tensile stresses in the different regions of the propellant grain at the end of the downward and upward thermal transients are summarized in Table 1. At the end of the upward thermal transient (60°C) the stress distribution is almost uniform throughout the motor. Even though the motor is close to its stress-free state at this temperature, some residual tensile stresses (100–120 kPa) remained from the previous cold cycle.

The deformed shape of the principal strain contours in the motor at the end of the downward and upward thermal transients are illustrated in Figs. 5a and b. The model for the upward thermal transient shows the inhibitor expanding and compressing against the propellant because of the higher thermal expansion coefficient of the inhibitor compared to the propellant at 60°C.[8] The maximum principal strains in the different regions of the propellant grain are listed in Table 1. The regions of highest maximum principal strains in the propellant grain are at the head end of the motor and also at the side adjacent to the holdback groove of the inhibitor. The critical regions of strain decrease with decreasing temperature. The regions of intense strain are smaller during the cold cycle compared to the hot cycle. Another region of high strain in the motor is in the small air gap between the inhibitor and insulation layers at the side of the motor (Fig. 1). The analysis showed that the air gap, being a poor conductor of heat, had some effect on the predicted stress distribution. During the temperature heating transient the propellant and inhibitor expand into the air gap and during cooldown the air gap opens up. This would have some effect on the magnitude and distri-

Table 1 Predicted stresses, strains and critical crack lengths in motor from viscoelastic and fracture analysis

Different regions of propellant grain	Thermal transient	von Mises stress, kPa	Maximum tensile principal stress, kPa	Maximum principal strain, %	Critical crack length, mm
Center of head end	25 to −40°C, after 2 h	180–200	60	0.6	5–6
Side, adjacent to holdback groove of inhibitor	——	180–200	60	1.2–1.3	8–10
Corner of dome	——	180–200	100	0.3–0.4	1
Center of head end	End of cold cycle (−40°C)	400–440	1200	0.7	2
Side, adjacent to holdback groove of inhibitor	——	400–440	1100	1.1–1.3	2
Corner of dome	——	400–440	1100–1200	0.8	0.3
Center of head end	End of hot cycle (+60°C)	110	100–120	1.4	10
Side, adjacent to holdback groove of inhibitor	——	140	100–120	1.4	10
Corner of dome	——	110	100–120	1.2	3–4

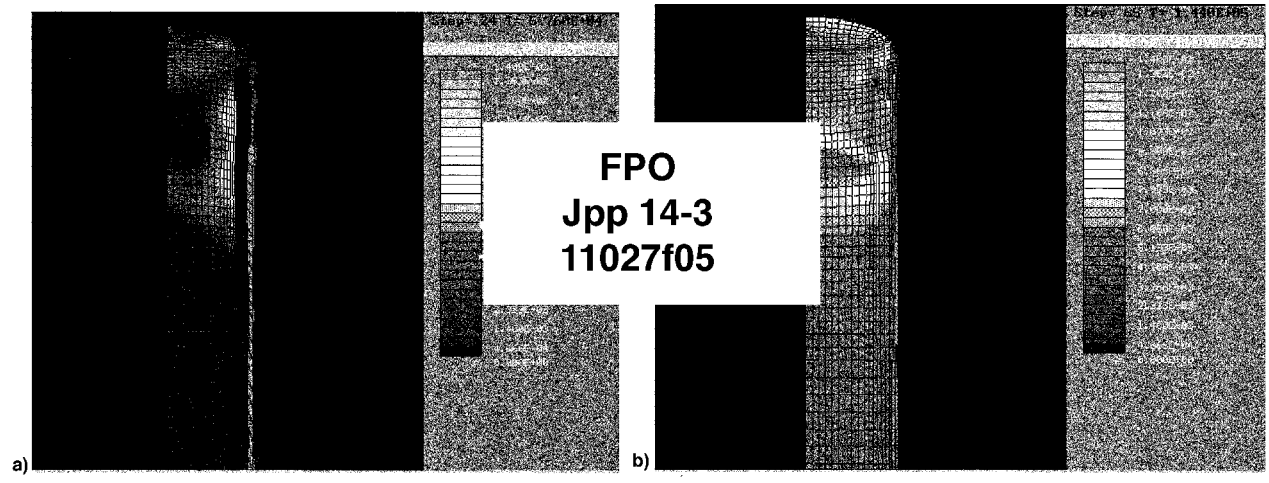

Fig. 5 Principal strain contours for a) end of downward (25 to −40°C) thermal transient and b) end of upward (25 to +60°C) thermal transient.

bution of the stresses and strains in the propellant during the transients.

The changes in propensity for crack propagation during one complete thermal shock cycle are shown in Figs. 6a–6f. The model predicts that after 1.3 h at −40°C (Fig. 6a), the region of highest propensity for crack propagation is at the corner of the dome in the propellant charge. The critical crack lengths decrease with time during the cold cycle. On equilibration to 25°C, the propensity for crack propagation decreases and critical crack lengths are longer. During the hot cycle at 60°C, the critical crack lengths decrease again but are longer than those at −40°C, i.e., the propensity for crack propagation is much higher at −40°C, where the motor encounters higher thermal loads. The critical crack lengths required for propagation, i.e., cracks will not propagate below this minimum value, for the different thermal transients are listed in Table 1. In the hot cycle, the critical crack lengths are 3–10 mm, whereas they are 0.2–2 mm in the cold cycle. Experimental observations from previous studies showed that the real crack propagation regions in this end-burning motor (subjected to similar thermal loadings as those used in the finite element analysis) matched the high-propensity regions calculated from the fracture analysis.[8,12] In these experiments, two uninstrumented Pictor motors were subjected to several thermal shock cycles and radiographed at the end of each cold and hot cycle. It should be noted that the thermal shock conditions (Fig. 2) were much more severe than what the motors would normally see in service to induce cracking. At the end of the first cold cycle, cracks were first visible at the corner of the dome at the head end of the motor, but they appeared to have closed up after the end of the first hot cycle. At the end of the fourth cold cycle, long axial cracks (4–11 cm) were visible at the head end of the motor near the propellant-inhibitor interface. In subsequent hot and cold cycles the cracks propagated and became more pronounced in the radiographs.

It should be noted that in the crack-propagation analysis it was assumed that the critical strain energy release rate does not vary very much from 25 to −40°C. Preliminary experimental data from this laboratory show that G_c for the propellant at −40°C is 1.2–1.5 times higher than the value at 25°C.[8,12] However, this does not alter the conclusions drawn from this study on the stress and strain distributions and the critical regions in the propellant grain for crack propagation. Also, the temperatures in the downward thermal transients used in this study were well above the glass transition temperature of −75°C for the propellant studied here, i.e., the analysis was run at temperatures above the brittle to ductile transition T_g and, therefore, failure modes are not expected to change. The capability to vary G_c with temperature in the finite element code is currently being implemented.

It is interesting to compare the critical regions in the propellant grain predicted by the various fracture/initiation criteria. Our results indicate that the critical regions for crack propagation are similar to the maximum tensile principal stress but are different to the von Mises stress distribution. This suggests that only the normal applied stress is effective in causing crack growth. For this motor geometry the regions of highest maximum principal strain are different to the regions of highest propensity for crack propagation. This is not unexpected because the maximum strains in this motor are less than 1.5% and fracture is likely to be stress induced rather than strain induced. However, this result may be different for a radial burner where the likely failure mode is cracking in the bore of the motor, which is strain induced. A similar viscoelastic and fracture analysis can be conducted on a radial burning motor to see if the regions of maximum principal strain cor-

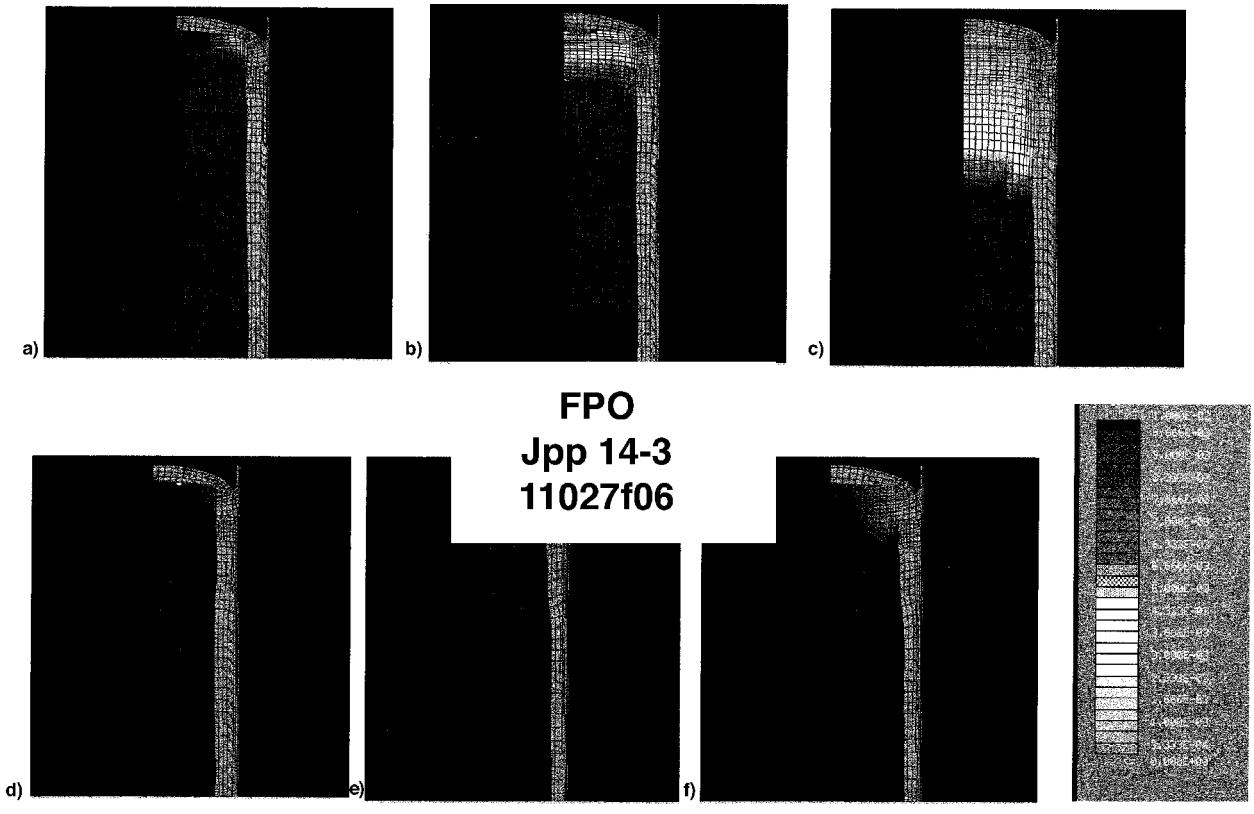

Fig. 6 Contours of propensity for crack propagation during thermal shock cycle after a) 1.3 h, beginning of cold cycle at −40°C; b) 2.7 h, −40°C; c) 8.7 h, −40°C; d) 22.7 h, end of equilibration at 25°C for 8 h; e) 32 h, 60°C; and f) 40 h, end of hot cycle at 60°C.

respond to the critical regions of crack propagation in the motor. The results from this study support the use of fracture energy as an alternative failure criterion, which appears to be a more complete failure criterion than criteria based on stress or strain capability alone.

Conclusions

A modified fracture mechanics approach, which accounts for bulk inelastic behavior in the calculation of the fracture energy, and a simple method for nonlinear viscoelastic analysis, where a three-dimensional interpolation scheme is used to solve the Prony series equations that represent the relaxation modulus as functions of time, temperature, and strain level, have been developed and implemented into a finite element code.

The method for nonlinear viscoelastic analysis appeared to be sufficiently accurate to predict the thermal stresses in an end-burning rocket motor. Reasonably good agreement between the stresses measured using miniature normal stress sensors embedded in the propellant grain and the predicted von Mises stresses were obtained. However, the effect of previous loading histories and, therefore, possible damage in the material, on the relaxation modulus have been neglected in the present study.

The fracture analysis predicted the minimum crack lengths below which propagation would not occur, and also the regions in the motor with high propensity for cracks to propagate under a thermal shock loading The critical regions in the propellant grain predicted by the various fracture/initiation criteria were compared. For both the upward and downward thermal transients, the regions of high propensity for crack propagation corresponded to the critical regions of maximum tensile principal stress in the motor, suggesting that only the normal applied stress is effective in causing crack growth. The maximum principal strain distributions did not match the critical regions for crack propagation; failure in this motor is not expected to be strain induced. A capability to vary G_c with temperature in the fracture analysis should give a more accurate prediction of the critical crack lengths at temperatures close to T_g, where G_c is significantly different to that at 25°C.

Acknowledgment

The authors acknowledge the assistance of S. Mitchell of G+D Computing Pty. Ltd., in performing the structural analysis work.

References

[1]Collingwood, G. A., Dixon, M. D., Clark, L. M., and Becker, E. B., "Solid Rocket Motor Service Life Prediction Using Nonlinear Viscoelastic Analysis and a Probabilistic Approach," *Proceedings of the 87th NATO/AGARD/PEP Symposium on Service Life of Solid Propulsion Systems* (Athens), AGARD, CP-586, 1996.

[2]Marsh, B. P., and Counter, M. S., "A Method of Service Life Prediction Using Linear Cumulative Damage Theory," U.S. Army Missile Command TR RD-PR-93-8, 1993.

[3]Thrasher, D. I., and Hildreth, J. H., "Structural Service Life Estimate for a Reduced Smoke Rocket Motor," *Journal of Spacecraft and Rockets*, Vol. 19, No. 6, 1982, pp. 564–570.

[4]Francis, E. C., and Thompson, R. E., "Nonlinear Structural Modelling of Solid Propellants," *Proceedings of the AIAA/SAE/ASME Joint Propulsion Conference* (Cincinnati, OH), AIAA, New York, 1984.

[5]Francis, E. C., Peters, R. L., and Hufferd, W. L., "Considerations in the Applications of Nonlinear Structural Materials," *Proceedings of 2nd International Conference on Mechanical Behaviour of Materials* (Boston, MA), 1976.

[6]Swanson, S. R., and Christensen, L. W., "A Constitutive Formulation for High Elongation Propellant," *Journal of Spacecraft and Rockets*, Vol. 20, No. 6, 1983, pp. 559–566.

[7]Ho, S. Y., and Tod, D. A., "Mechanical Failure Analysis of Rubbery Composite Propellants Using a Modified Fracture Mechanics Approach," *Proceedings of the 21st International Conference of ICT* (Karlesruhe, Germany), 1990, pp. 1–14 (Paper 30).

[8]Ho, S. Y., Ide, K., and Macdowell, P., "Instrumented Service Life Program for the Pictor Rocket Motor," *Proceedings of the 87th NATO/AGARD/PEP Symposium on Service Life of Solid Propulsion Systems* (Athens), 1996.

[9]Liu, C. T., "Microstructural Damage and Crack Growth Behaviour

in a Composite Solid Propellant," *Proceedings of the 87th NATO/AGARD/PEP Symposium on Service Life of Solid Propulsion Systems* (Athens), 1996.

[10]Kinloch, A. J., and Tod, D. A., *Propellants, Explosives, Pyrotechnics*, Vol. 9, 1984, pp. 48–55.

[11]Kinloch, A. J., and Young, R. J., *Fracture Behaviour of Polymers*, Elsevier, London, 1983.

[12]Ho, S. Y., and Macdowell, P., "New Service Life Methodologies for Solid Propellant Rocket Motors," Aeronautical and Maritime Research Lab., DSTO Research Rept. DSTO-RR-0099, Melbourne, Australia, April 1997.

[13]Kinloch, A. J., and Gledhill, R. A., *Journal of Spacecraft and Rockets*, Vol. 18, No. 4, 1981, pp. 333–337.

[14]Stevens, G., Carè, G., and Mitchell, S., G+D Computing Pty. Ltd., TR 0196-1P, Sydney, Australia, March 1996.

[15]"STRAND 6 Finite Element Analysis System Reference Manual and User Guide" G+D Computing Pty. Ltd., Sydney, Australia, 1993, p. 483.

Color reproductions courtesy of the Aeronautical and Maritime Research Laboratory.